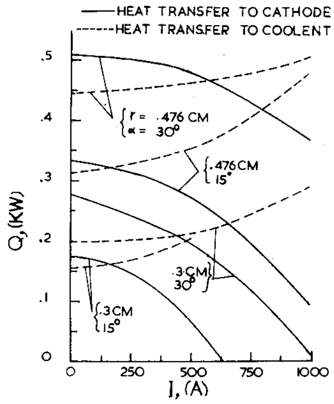

Fig. 3 Heat transfers to cathode and to coolant vs applied current.

$r=0.3$ and 0.476 cm, $\alpha=15$ and 30 deg are depicted in Fig. 2. It is seen that temperature decreases rapidly along the nosecone portion of the cathode ($0 \leq X \leq X_l$), while in the remaining length of the cathode ($X_l \leq X \leq 1$), the temperature varies almost linearly. The decrease in α increases the electrical resistance due to the decrease in the cross-sectional area in the nosecone portion of the cathode. However, it is found that numerical instability occurs for $r=0.3$ cm at $I>500$ A and $\alpha=15$ deg and also at $I>1000$ A and $\alpha=30$ deg. This numerical instability is attributed to overheating of the cathode root by Joule's heating when the current exceeds the above values. Figure 3 shows the variation of Q_s and Q_0 as a function of applied current. It is interesting to note that as current increases, heat transfer to cathode coolant increases, while heat transfer to cathode tip decreases rapidly and reaches to zero value at the point where the numerical instability is noticed in the computations. It can be concluded, therefore, that for $I<500$ A, a small diameter and small semicone angle of cathode is economical, owing to less heat transfer to coolant, while $I>500$ A, a larger diameter, and short nosecone length of cathode is favorable in order to prevent melting of the cathode tip due to excessive Ohmic heating. It would be worthwhile to mention here that the characteristic cathode voltage $U_c (=Q_s/I)$ decreases with increasing arc current, while heat transfer to the cathode coolant increases with increasing arc current, as shown in Fig. 3. This is very similar to the trend observed by conventional experiments on an MPD arc.[5]

At the cathode the electron component has to satisfy the appropriate emission law. It would be inappropriate to discuss electron emission theories here. However, it is sufficient to mention that a theory of thermionic emission under the influence of high temperature has been developed by Richardson.[11] The expression for current density can be written as

$$j=AT^2\exp(-b/T) \tag{3}$$

where A and b are constants[11] and T is cathode temperature.

For the sake of brevity, we are not presenting the current density profile along the cathode. Integration of Eq. (3) over the cathode surface yields a value of total discharge current from cathode to arc. Using thermionic relation only, 70-85% current continuity condition is satisfied at the cathode root. In order to satisfy current continuity condition precisely one has to take into consideration the combined effect of thermionic and field emission in computation of current density profile along the cathode and also higher cathode tip temperature.

One disadvantage of invoking the numerical analysis is that the results do not give a clear functional relation among the arc current density and temperature at the cathode root vs cathode geometrical configuration. The following simple procedure may be adopted for computational purposes in the thermal design of the cathode:

1) Select the primary cathode geometrical configuration from Fig. 3 for a given value of applied current.

2) Satisfy the current continuity condition by taking into account thermionic and field emission expressions. If the desired accuracy is not achieved, change the geometrical parameters or cathode tip temperature or both and solve Eqs. (2) to obtain temperature distribution along cathode.

3) Repeat the preceding steps until the current continuity condition satisfies a given limit of tolerance.

References

[1] Malliaris, A. C., "Phenomena in the Cathode Region of an MPD Accelerator," *AIAA Journal*, Vol. 5, July 1967, pp. 1325-1328.

[2] Turchi, P. J. and John, R. G., "Cathode Region of a Quasi-Steady MPD Arc Jet," *AIAA Journal*, Vol. 9, July 1971, pp. 1372-1379.

[3] Lee, T. H., Greenwood, A., Breingan, W. D., and Fullerton, H. P., "Voltage Distribution, Ionization, and Energy Balance in the Cathode Region of an Arc," ARL 64-152, Office of Aerospace Research, Wright-Patterson AFB, Ohio, Oct. 1964.

[4] Mehta, R. C., "Theoretical Analysis of Constricted Electric Arc by Iteration Method," *Journal of Applied Physics*, Vol. 50, June 1979, pp. 4453-4456.

[5] Shih, K. T., Pfender, E., and Eckert, E.R.G., "Thermal Analysis of Cathode and Anode Regimes of an MPD Arc," NASA CR 54664, Jan. 1968.

[6] Emmons, H. W., "Recent Development in Plasma Heat Transfer," *Modern Development in Heat Transfer*, Academic Press, New York, 1963, pp. 401-478.

[7] Donskoi, A. V., Klubrikin, V. S., and Parkhomenko, A. S., "The Effect of Arc Length on the Electrical Characteristics of a Plasmatron," *High Temperature*, Vol. 8, May-June 1970, pp. 461-465.

[8] Olsen, H. N., "Determination of Properties of an Optically Thin Argon Plasma," *Temperature, Its Measurement and Control in Science and Industry*, Vol. III, Part 1, C. M. Herzfeld, ed., Reinhold Publishing Corp., New York, 1972.

[9] Eckert, E.R.G. and Drake, R. M., *Analysis of Heat and Mass Transfer*, McGraw Hill Book Co., Inc., New York, 1972.

[10] *Standard Handbook for Electrical Engineering*, 9th Ed., McGraw Hill Book Co., Inc., 1957, p. 478.

[11] Cobine, J. D., *Gaseous Conductor*, Dover Publication Inc., New York, 1958, pp. 106-122.

Modal Analysis of the Transient Asymmetric Response of Thin Circular Plates

H. D. Fisher*

Combustion Engineering, Inc., Windsor, Conn.

Introduction

SCHLAK et al[1] have presented a general integral solution for the free and forced response of an elastically supported, thin circular plate subjected to a time-dependent surface load. The generalized theory contained in Ref. 1 encompasses the axisymmetric analysis of Weiner[2] which was corrected by Fisher.[3] An attempt to derive the equations governing the axisymmetric plate response to a concentrated central loading from the general solution of Ref. 1 has disclosed that three of the equations contained in Ref. 1 are incorrect.

The objectives of this Note are to: 1) indicate the corrections required in the section of Ref. 1 entitled General Analysis, 2) compare the transient deflection histories from

Received Feb. 27, 1979; revision received May 7, 1979.

Index category: Structural Dynamics.

*Consulting Engineer, Reactor Engineering Dept.

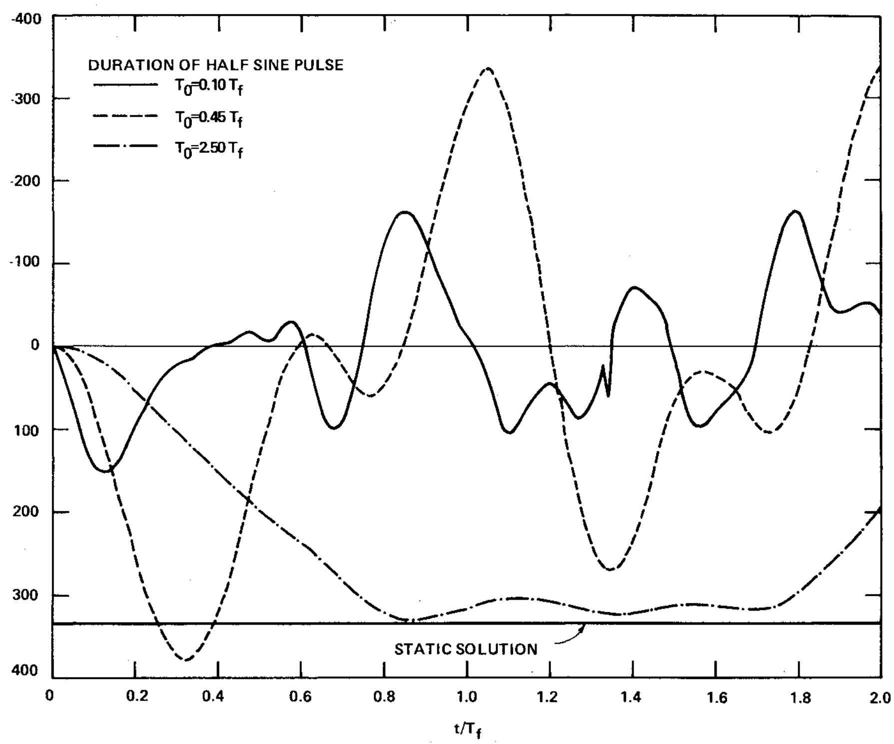

Fig. 1 Plate response at $\theta = 0$ and $R = 0.5$.

the present formulation with those in Fig. 3 of Ramakrishnan and Kunukkasseril,[4] 3) demonstrate agreement between the maximum deflection resulting from quasistatic loading with the corresponding deformation given in Timoshenko.[5]

Analysis

Comparison of Ref. 1 with Refs. 2, 6, and 7 discloses that Eq. (14) of Ref. 1 should be replaced by

$$Q_{mos} = 0 \qquad Q_{moc} = 2\pi \int_0^a r R_{mn}^2(r)\,\mathrm{d}r \qquad (14a)\dagger \qquad (1)$$

$$Q_{mns} = Q_{mnc} = \pi \int_0^a r R_{mn}^2(r)\,\mathrm{d}r \qquad (14b) \qquad (2)$$

The quantity Q_{mn} appears in Eqs. (13) and (17) of Ref. 1. It should be replaced by Q_{mns} in Eq. (13) and Q_{mnc} in Eq. (17).

This result follows since

$$\int_0^{2\pi} \sin^2 n\theta \mathrm{d}\theta = 0 \qquad \int_0^{2\pi} \cos^2 n\theta \mathrm{d}\theta = 2, \quad n = 0$$

$$\int_0^{2\pi} \sin^2 n\theta \mathrm{d}\theta = \int_0^{2\pi} \cos^2 n\theta \mathrm{d}\theta = \pi, \quad n \neq 0 \qquad (3)$$

Equation (15) of Ref. 1 should read

$$\begin{aligned}\int_0^a R_{mn}^2(r) r\mathrm{d}r &= a^2 [J_n^2(\alpha_{mn}) - (1 - \alpha_{mn}^2/\gamma_{mn}^2) \\ &\times \{(1/2) J_{n+1}^2(\alpha_{mn}) + J_{n+1}(\alpha_{mn}) J_n'(\alpha_{mn})\}] \\ &- [a^2/(1-\nu-k_2 a/D)][\{2 + (\alpha_{mn}^2 + \gamma_{mn}^2)^2 \\ &/[2\gamma_{mn}^2(1-\nu-k_2 a/D)]\} J_n^2(\alpha_{mn}) \\ &+ (\alpha_{mn}/\gamma_{mn}^2)(\alpha_{mn}^2 + \gamma_{mn}^2) J_n(\alpha_{mn}) J_n'(\alpha_{mn})] \qquad (15a) \qquad (4)\end{aligned}$$

†In the case of two numbers for the same equation, the first number refers to Ref. 1 and the second is the required numbering in the present text.

Equation (4) may be recast as

$$\begin{aligned}\int_0^a R_{mn}^2(r) r\mathrm{d}r &= (a^2/2)[J_n^2(\alpha_{mn}) - \{(2n/\alpha_{mn}) J_n(\alpha_{mn}) \\ &- J_{n+1}(\alpha_{mn})\} J_{n+1}(\alpha_{mn})] - 2a^2 J_n(\alpha_{mn}) \\ &\times \{\alpha_{mn} J_{n+1}(\alpha_{mn}) I_n(\gamma_{mn}) + \gamma_{mn} J_n(\alpha_{mn}) I_{n+1}(\gamma_{mn})\} \\ &/\{(\alpha_{mn}^2 + \gamma_{mn}^2) I_n(\gamma_{mn})\} + (a^2/2)[J_n^2(\alpha_{mn})/I_n^2(\gamma_{mn})] \\ &\times [I_n^2(\gamma_{mn}) - \{(2n/\gamma_{mn}) I_n(\gamma_{mn}) \\ &+ I_{n+1}(\gamma_{mn})\} I_{n+1}(\gamma_{mn})] \qquad (15b) \qquad (5)\end{aligned}$$

Equation (5) was first derived in Ref. 6. For $\alpha_{mn} = \gamma_{mn}$ and $k_1 = 0$, special cases of the norm given in Eqs. (4) and (5) have been derived previously as follows: 1) axisymmetric loading of an elastically restrained plate—Eq. (25) of Ref. 2; 2) asymmetric loading of a simply-supported circular plate—Eq. (108) of Ref. 7; 3) asymmetric loading of a clamped, circular plate—Eq. (8) of Ref. 4.

With the exception of Ref. 7, which contains a sign error, the norms in cases 1, 2, and 3 above are identical (within a multiplicative constant due to the variation in the normalization of the eigenfunctions in the various problems) to those given by Eqs. (4) and (5).

Numerical Example

The problem chosen for investigation is a half-sine concentrated-impact load applied to a clamped circular plate midway between the center and the clamped boundary. This loading and boundary condition were investigated in Ref. 4, where amplitudes and durations of 13.05 kg, 0.5 ms; 14.36 kg, 2.25 ms; and 22.6 kg, 12.5 ms were specified to obtain the three solutions presented in Fig. 3 of Ref. 4. The required loading representation for use with the formulation contained in Ref. 1. is

$$p(r,\theta,t) = P\delta(r - r_0)\delta(\theta - \theta_0)(1/r)\sin\omega t, t \leq \pi/\omega$$

$$p(r,\theta,t) = 0, \quad t > \pi/\omega \qquad (6)$$

Table 1 Frequencies vs mode numbers

Number	Ω^a (this analysis)	Ω^a (Ref. 4)	n^b	m^b
1	3.1962	3.1960	0	0
2	4.6109	4.6110	1	0
3	5.9057	5.9057	2	0
4	6.3064	6.3064	0	1
5	7.1435	7.1435	3	0
6	7.7993	7.7993	1	1
7	8.3466	8.3466	4	0
8	9.1969	9.1969	2	1
9	9.4395	9.4395	0	2
10	9.5257	9.5257	5	0
11	10.5367	10.5367	3	1
12	10.6870	10.6870	6	0
13	10.9581	10.9581	1	2
14	11.8345	11.8345	7	0
15	11.8367	11.8367	4	1
16	12.4022	12.4022	2	2
17	12.5771	12.5771	0	3
18	12.9709	12.9770	8	0
19	13.1074	13.1074	5	1
20	13.7951	13.7951	3	2
21	14.0981	14.1086	9	0
22	14.1086	15.5795	1	3
23	14.3552	15.7164	6	1
24	15.1499	17.2557	4	2
25	15.2175	18.7440	10	0
26	15.5795	18.8565	2	3
27	15.5846	20.4010	7	1
28	15.7164	21.9977	0	4
29	16.3303	23.5453	11	0
30	16.4751	25.1379	5	2

[a] Ω defined in Eq. (5) of Ref. 1. [b] n and m correspond to frequencies determined in this analysis.

where P is the applied concentrated load.

Note that a comparison of Eq. (6) with Eq. (25) of Ref. 1 demonstrates that the factor of $(1/r)$ has been omitted from the right-hand side of the latter equation. Results obtained in the present analysis for the above half-sine pulses are plotted in Fig. 1 using the dimensionless variables introduced in Ref. 4. The variables associated with the ordinate are $W=\bar{W}/\bar{a}$ and $P=\bar{P}/(\bar{a}C)$ with the $\bar{W}$ the transverse displacement, $\bar{P}$ [not P as in Eq. (6)] the applied concentrated load, $\bar{a}$ the plate radius, and c the extensional rigidity. P is defined incorrectly in the Appendix of Ref. 4, but was subsequently defined as given above the Kunukkasseril and Chandrasekharan.[8] The abscissa is obtained by dividing the elapsed time by the period of the fundamental mode of the plate ($T_f=5.03\times10^{-3}$ s). Due to the normalization by the applied concentrated load, the static solution from Ref. 5, shown as a solid horizontal line in Fig. 1, is identical for these three loadings. The discrepancies between Figs. 1 and Fig. 3 of Ref. 4 are attributed to:

1) The use of the incorrect normalization condition

$$\int_0^{2\pi}\int_0^1 W_{nm}^2 r\mathrm{d}r\mathrm{d}\theta=\pi$$

in Eq. (8) of Ref. 4 instead of that given by Eq. (3).

2) The omission of several modes in the tabulation of the first 30 modes given in Table 1 of Ref. 4. For comparison, the lowest 30 modes employed in the present analysis as well as those given in Ref. 4 are tabulated in Table 1.

The effect of increasing the number of modes in the solution from 30 to 60 is barely perceptible (the curves of Fig. 1, where the 60-mode solutions are plotted, are changed by less than 1%). As a further check on the solution, the 22.6-kg load was applied in the quasistatic manner by specifying the dimensionless duration of impact as $(1\times10^7)t/T_f$. As required, the maximum response occurred at $t/T_f=0.5\times10^7$ and was 0.99 of that given by Ref. 5.

Acknowledgment

Development of the computer program required in this analysis was funded by a project under the direction of H. A. Runde.

References

[1] Schlack, A. L., Kessel, P. G., and Dong, W. N., "Dynamic Response of Elastically Supported Circular Plates to a General Surface Load," *AIAA Journal*, Vol. 10, June 1972, pp. 733-738.

[2] Weiner, R. S., "Forced Axisymmetric Motions of Circular Elastic Plates," *Journal of Applied Mechanics*, Vol. 32, 1965, pp. 893-898.

[3] Fisher, H. D., "Modal Coefficients for the Axisymmetric Response of Thin Circular Plates," *Journal of Applied Mechanics*, Vol. 43, 1976, pp. 511-513.

[4] Ramakrishnan, R. and Kunukkasseril, V. X., "Asymmetric Response of Circular Plates," *Journal of Sound and Vibration*, Vol. 34, 1974, pp. 489-504.

[5] Timoshenko, S., *Theory of Plates and Shells*, Second Ed., McGraw-Hill, N.Y., 1959, p. 293.

[6] Chonan, S., "Random Vibration of an Elastically Supported Circular Plate with an Elastically Restrained Edge and an Initial Tension," *Journal of Sound and Vibration*, Vol. 58, 1978, pp. 443-454.

[7] Anderson G., "On the Determination of Finite Integral Transforms for Force Vibrations of Circular Plates," *Journal of Sound and Vibration*, Vol. 9, 1969, pp. 126-144.

[8] Kunukkasseril, V. X. and Chandrasekharan, K., "Concentrated-Impact Loading of Circular Plates," *Experimental Mechanics*, Nov. 1975, pp. 424-428.

Effect of Nonhomogeneity in Orthotropic Curved Plates

Nicos M. Patsalides* and Thomas J. Kim†
University of Rhode Island, Kingston, R.I.

Introduction

IN the design of fiber-reinforced plastic structures, it is often necessary to use fibers with different modulus and strength properties (mixing and matching method) in order to minimize the extreme fiber stress. Curved members of uniform thickness and such type of mixed fiber structure may then be approximated by radially nonhomogenous orthotropic curved plates. The problem of an orthotropic homogenous plate was first attempted by Carrier.[1] Later, Bert[2] and Shaffer[3,4] obtained the general solutions for nonhomogenous disks and tubes. Using linear elasticity theory, Griffin[5] studied the bending behavior of an isotropic homogenous thick curved plate due to edge loadings, and compared his results with elementary theory.

In this paper, the bending behavior of a nonhomogenous orthotropic curved plate subjected to surface tractions and edge forces is investigated. The layered fiber reinforcement in the plate is assumed to be radially nonhomogenous and orthotropic, and the Airy's stress function approach is used.

Analysis

The stress-strain relations for an orthotropic and radially nonhomogenous elastic material can be written in the form[6]:

$$\epsilon_r=a_{11}\sigma_r+a_{12}\sigma_\theta,\quad \epsilon_\theta=a_{12}\sigma_r+a_{22}\sigma_\theta,\quad \gamma_{r\theta}=a_{66}\tau_{r\theta} \tag{1}$$

Received Nov. 2, 1978; revision received April 26, 1979.

Index category: Structural Statics.

*Engineer, Gulf & Western Energy Products Group.
†Professor.